Low-temperature-grown GaAs: modeling of transient reflectivity experiments

V. Ortiz, J. Nagle, Jean-Francois Lampin, Emmanuel Peronne, Antigoni Alexandrou

Low-temperature-grown GaAs: Modeling of transient reflectivity experiments

Cite as: J. Appl. Phys. **102**, 043515 (2007); https://doi.org/10.1063/1.2763971
Submitted: 12 February 2007 • Accepted: 13 June 2007 • Published Online: 23 August 2007

V. Ortiz, J. Nagle, J.-F. Lampin, et al.

Low-temperature-grown GaAs: Modeling of transient reflectivity experiments

V. Ortiz and J. Nagle
Thales Research & Technology, Route Départementale 128, 91767 Palaiseau, France

J.-F. Lampin
Institut d'Electronique, de Microélectronique et de Nanotechnologies, CNRS UMR 8520, Av Henri Poincaré, Villeneuve d'Ascq, France

E. Péronne[a)]
Laboratoire d'Optique Appliquée, ENSTA, Ecole Polytechnique, CNRS UMR 7639, 91761 Palaiseau, France
and Laboratory for Optics and Biosciences, Ecole Polytechnique, CNRS UMR 7645, INSERM U696, 91128 Palaiseau, France

A. Alexandrou
Laboratory for Optics and Biosciences, Ecole Polytechnique, CNRS UMR 7645, INSERM U696, 91128 Palaiseau, France

(Received 12 February 2007; accepted 13 June 2007; published online 23 August 2007)

A simple nonradiative Shockley-Read-Hall recombination model is used to interpret transient reflectivity and midinfrared transmission experiments of low-temperature-grown GaAs (LT-GaAs) materials annealed under various conditions of temperature and duration. The model introduces two main parameters, namely the deep-donor (N_{DD}) and the acceptor (N_A) concentrations in the GaAs matrix, to explain all observed behaviors coherently with other results in the literature. A precise study of the different parameters (pump wavelength and power, N_{DD}, N_A, etc.) is performed using our model. The introduction of growth and anneal-related parameters, such as N_A and N_{DD}, allows a good understanding of LT-GaAs. These results demonstrate the importance of acceptor densities in the dynamic properties. © *2007 American Institute of Physics*. [DOI: 10.1063/1.2763971]

I. INTRODUCTION

Low-temperature-grown GaAs (LT-GaAs) is a key constituent for ultrafast optical and optoelectronic components, such as THz radiation sources/detectors or semiconductor saturable absorber mirrors for femtosecond pulse generation. This is related to the material's very short carrier lifetime, which is on the order of 0.1–10 ps, combined with a high carrier mobility, which ranges from 10 to 1000 $cm^2/V\,s$. However, in spite of several years of study and the importance of LT-GaAs for the above-mentioned emerging technologies, much of its basic properties still need a better understanding. This is particularly the case if one wants to perform a "fine-tuning" of the LT-GaAs properties in order to optimize a given device.

It is known that during the growth of LT-GaAs, an important amount of As-related point defects (As interstitials or antisites, Ga vacancies) is incorporated into the matrix.[1] The antisite (As_{Ga})-related defects are known to form a deep-donor (DD) band, which is partially ionized by residual acceptors incorporated during the growth (like carbon) or by gallium vacancies (V_{Ga}) incorporated during the LT growth, which are known to be acceptors.[2,3] The partially ionized DD band forms an effective recombination center, which lowers the carrier lifetime to the picosecond range without decreasing dramatically the mobility. When the material is annealed, the point defects precipitate into As clusters, which usually leads to an increase of the carrier lifetime and a recovery of the mobility. The resistivity and carrier lifetime of LT-GaAs have been shown to depend critically on post-growth annealing conditions.[4–10]

Carrier lifetime measurements are performed using various techniques, such as pump-probe reflectivity,[6–9,11,12] pump-probe transmission,[4,13] or photoconductive sampling.[14] Concerning the interpretation of the measured carrier lifetimes and the capability of predicting them, however, there is still a lack of quantitative analysis covering the entire range of the possible treatments of the material, from the as-grown situation to the different possible annealings. Previous rate-equation models used to describe the dynamic properties of LT-GaAs layers have the disadvantage of using parameters that cannot be easily related to basic material properties (such as acceptor or donor concentrations). In Ref. 12, we presented the advantages of a one-center Shockley-Read-Hall (SRH) rate equation model to calculate the different carrier concentrations as a function of time. The study showed that, for the samples studied, the negative transients observed in photoreflectivity experiments were related to the amount of acceptors present in the LT-GaAs matrix.

Here, we perform a systematic analysis of the transient photoreflectivity and infrared (IR) transmission data taken from various LT-GaAs layers grown at different temperatures

[a)]Present address: Institut des NanoSciences de Paris, University Paris 6 and Paris 7, CNRS UMR 7588, Campus Boucicaut, 140 rue de Lourmel, 75015 Paris, France.

(low and high) and annealed under different conditions (long and short cycles). These results are completed by a careful study of the effects of the model parameters.

This paper is organized as follows: (i) we detail precisely the experimental techniques used, including the calibration methods used during the molecular beam epitaxy (MBE) growth, and the pump-probe setup; (ii) we describe the results obtained with the different LT-GaAs samples; (iii) we detail the SRH model and the reflectivity curves calculation used to describe the experimental data; (iv) we perform a precise and exhaustive analysis of the recorded data using our model, relating the different parameters to quantifiable material properties.

II. EXPERIMENTAL TECHNIQUE

The samples studied (noted *A* and *B*) were grown on a Varian Mod Gen II MBE reactor, on epiready nominal semi-insulating GaAs (001) substrates. They consist of a 2 μm-thick layer of LT-GaAs embedded between 20-nm-thick $Al_{0.25}Ga_{0.75}As$ layers, in order to avoid surface recombination and leakage of photogenerated carriers to the substrate. These $Al_{0.25}Ga_{0.75}As$ layers provide efficient potential barriers for both electrons and holes created in the GaAs layer. In the absence of a cap layer, the carrier lifetime can be significantly reduced by surface recombination processes. The choice of this sample structure leads to a simplification of the theoretical analysis of the carrier dynamics since surface recombination can be neglected. We used an arsenic cracker cell to provide the As_4 flux, and controlled the V/III ratio with As_4 and Ga beam equivalent pressure measurements. To determine the V/III ratio, we took as a definition that, on a (100) GaAs substrate maintained at 550 °C, the surface reconstruction transition from the (2×4) to the (4×2) occurs for As/Ga=1. The growth rate of GaAs ($\sim$1 μm/h) was determined by the intensity oscillations of the specular reflection high-enery electron diffraction (RHEED) beam from GaAs (100) substrates. The surface temperature above 400 °C was measured by a short- wavelength (0.94 μm) pyrometer. For temperatures below 400 °C (i.e., for LT-GaAs growth), the substrate temperature was estimated with a thermocouple placed behind the substrate. The thermocouple temperature is not a parameter that can be compared between different growth reactors or even different kinds of substrates. We therefore took the following precautions: we used the same molybdenum substrate holder as well as the same kind of substrates (2 in., semi-insulating, and single face polished). We furthermore used the deep-donor (DD) concentration as the main parameter to characterize the grown LT-GaAs layers. Indeed, the deep-donor concentration is related to the excess As incorporated in the matrix and can be measured by high-resolution x-ray diffraction (HR-XRD). For samples *A* and *B*, a V/III ratio of 2.2 was used. The thermocouple temperatures were 280 and 320 °C for the samples *A* and *B*, respectively. These temperatures correspond to the range of maximum practical interest when aiming at materials with short capture times and short recovery times. For higher growth temperatures, excess As concentrations are not large enough to produce very short capture times. For lower growth temperatures, there are slow recovery transients regardless of the annealing conditions.

Once grown, the samples were cleaved and flash-annealed for 500 °C/60 s, 700 °C/60 s, 800 °C/60 s, or 500 °C/600 s, under a N_2 atmosphere, face down on a GaAs substrate. HR-XRD analysis performed on all samples gave the lattice variation parameter $\Delta a/a$ induced by the excess arsenic incorporated in the layers. Using the calibration of Liu *et al.*,[15] we were able to estimate the DD concentration in our samples. We should note that for samples annealed above 700 °C, the DD concentration is below our detection limit ($\sim10^{18}$ cm^{-3}).

The pump-probe reflectivity experiments were performed at room temperature, using a femtosecond 76-MHz Ti:sapphire oscillator operating at 812 nm, with a full width at half-maximum duration of 100 fs. The pump beam of 70 mW, focused down to 50 μm, is expected to generate about 7×10^{17} cm^{-3} electron-hole pairs in the region probed by the reflected beam at the surface of the sample. In this configuration, the variation of the reflectivity as a function of the delay time between the pump and the probe at the same wavelength was measured. The transient reflectivity signal reflects the presence of carriers in the conduction and valence band: the photocreated carriers induce a change of absorption due to band filling, band-gap renormalization, trap filling state, and free-carrier absorption.[16] The measured $\Delta R/R_0$ signal is on the order of a few 10^{-4}.

The pump-probe transmission experiments were similar to the reflectivity ones, but although the pump was always at $\sim$812 nm, the probe was centered at 13 μm, i.e., 95 meV. For these experiments, we used a Ti:sapphire 200-kHz regenerative amplifier (Coherent) followed by a parametric amplifier and difference frequency mixer.[17,18] At this low probe energy (95 meV), neither gallium vacancies nor deep donors are excited because they have larger binding energies,[19] and even if shallow impurities or defect complexes exist with binding energy around or inferior to 95 meV, they are expected to be few in number. Moreover, since the Fermi level should be pinned to the DD band,[15,20] these shallow levels should be almost empty in the absence of laser pulse and thus contribute negligibly to the absorption. The transient repopulation of these levels during the pulse can also be neglected as long as the number of shallow levels is much smaller than the number of deep donors. When this holds, the measured IR transmission signal can be directly related to free-carrier absorption (either of electrons or holes).

III. EXPERIMENTAL RESULTS

Table I shows the DD concentrations determined from the HR-XRD or deduced afterwards from the fit (normal or italic characters, respectively). We can see that, as expected, the DD concentration is higher when the growth temperature is lowered, indicating an increase of the As-related defect incorporation for lower temperatures and thus a greater lattice parameter increase. Also, we observe a decrease of the DD concentration with the annealing, which reflects the precipitation and the As-cluster formation, with the consequent reduction of the amount of point defects in the matrix.

TABLE I. Sample parameters and growth conditions. For N_{DD}, normal characters: measured. For N_{DD} and all N_A values, italic characters: deduced from the fit.

	Anneal	N_{DD} (cm^{-3})	N_A (cm^{-3})
Sample *A*	as-grown	5.9×10^{19}	1.5×10^{18}
T_g=280 °C	500 °C/60 s	1.5×10^{19}	1.6×10^{18}
	700 °C/60 s	8.9×10^{17}	8.9×10^{17}
	800 °C/60 s	$(8-4.6)\times10^{17}$	4.6×10^{17}
	500 °C/600 s	1.0×10^{19}	7×10^{18}
Sample *B*	as-grown	2.3×10^{19}	5×10^{17}
T_g=320 °C	500 °C/60 s	6.7×10^{18}	7.5×10^{17}
	700 °C/60 s	$(8-5)\times10^{17}$	5×10^{17}
	800 °C/60 s	$(8-5.2)\times10^{17}$	5.2×10^{17}
	500 °C/600 s	5×10^{18}	4.2×10^{18}

Concerning the lifetimes, Figs. 1 and 2 show the recorded $\Delta R/R_0$ signal of samples *A* and *B* as a function of the pump-probe delay. Transient reflectivity data are presented on a linear scale in Fig. 1 and on a logarithmic scale in Fig. 2. We can see that the $\Delta R/R_0$ signal rapidly increases from zero to a maximum value as the pump injects electron-hole pairs into the LT-GaAs material. The signal then rapidly decreases in the following 0.5 ps. This is attributed to relaxation and cooling of the carriers, which are generated with a total excess energy of 120 meV above the band gap. The following nonexponential decrease of the signal corresponds to the carrier trapping by the DD states, which is usually related to the carrier lifetime.

In the data taken from as-grown samples [Figs. 2(a) and 2(b)], we observe a decrease of the decay time as the growth temperature decreases. This can be related to the increasing point-defect concentration (see Table I). Nevertheless, in the annealed 500 °C/60 s case, even if the DD concentration is decreased, two different behaviors are observed: for sample *A*, the lifetime remains almost unchanged compared to the as-grown case, while for sample *B*, the lifetime decreases significantly. This is inconsistent with the usual analysis, which assumes that the lifetime is inversely proportional to the amount of DD defects in the matrix.[7] However, for the 700 °C/60 s anneal, the lifetime becomes longer for both samples, and follows the expected behavior.

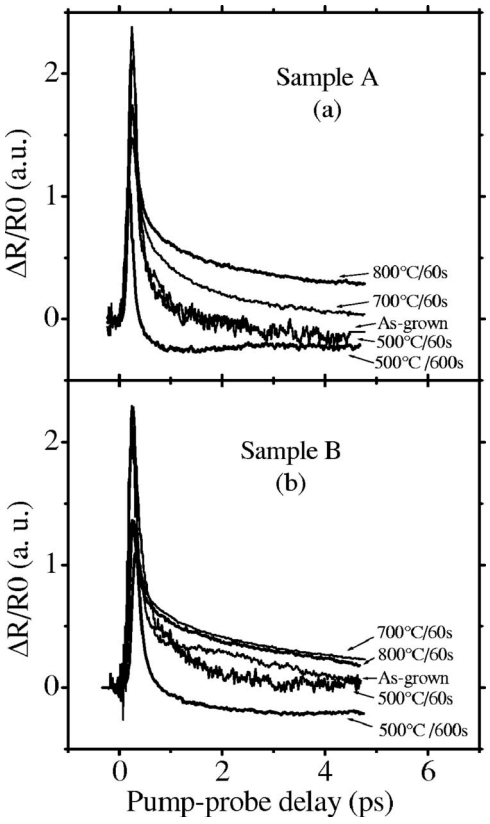

FIG. 1. Transient reflectivity signals (linear scale) recorded for sample *A* and sample *B* as-grown and after various annealing conditions.

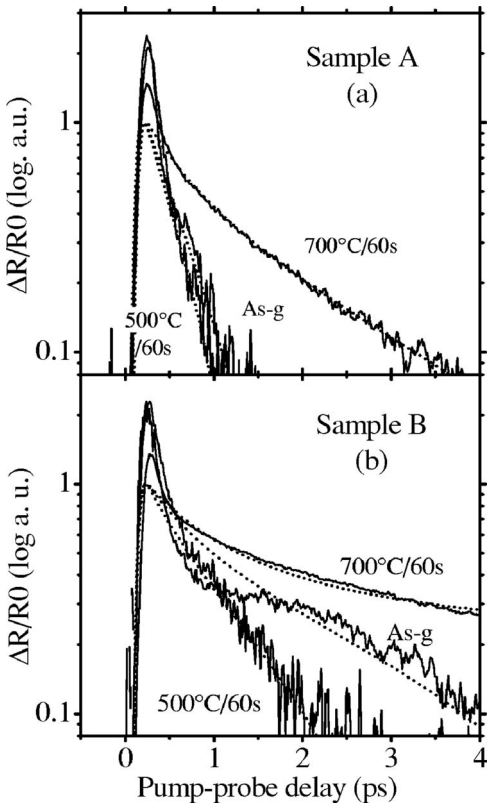

FIG. 2. Transient reflectivity signals (log scale) for sample *A* (top) and sample *B* (bottom) as-grown and annealed 60 s for 500 and 700 °C (solid lines) and their respective modeling (dotted lines).

Figure 3 shows results from both $\Delta R/R_0$ and $\Delta T/T_0$ IR measurements for sample *B* annealed 500 °C/600 s. It is important to note that the same pump intensity was used for both measurements. Two different behaviors can be observed: while the $\Delta R/R_0$ signal has a first very fast, subpicosecond decrease followed by a negative, very long (~100 ps) recovery time, the $\Delta T/T_0$ IR signal has only a single very slow decrease with a time constant of ~150 ps.

Figure 4 shows the recorded transient reflectivity data taken from samples annealed 800 °C/60 s. The decay rate is, as expected, longer than for the as-grown cases, but surprisingly, the decay rate for sample *B* annealed 800 °C/60 s is similar or even slightly shorter than for sample *B* annealed 700 °C/60 s (see Fig. 1). We should note that for the 800 °C/60 s anneal, we were unable to determine the N_{DD} using the x-ray diffraction analysis, which is under our detection limit, but we would not expect an increase of this

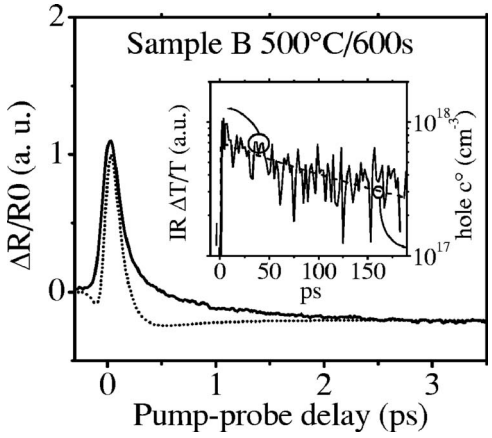

FIG. 3. Transient reflectivity signal for sample *B* annealed 500 °C/600 s (solid) and its respective simulation (dotted). Inset: Infrared transient transmission signal for the same sample (solid) and hole density deduced from the same simulation (dotted). The decay rate is the same for both curves.

value with an increased annealing temperature. The decrease of the decay rate with temperature should therefore not be related to an increase of N_{DD}.

These results show the following. First, the observed decay rates do not follow the reduction of the N_{DD} concentration in the samples, which seems to contradict the recombination model generally accepted for LT-GaAs. Second, the slow or long-lasting negative transients (NTs) observed cannot be explained in terms of a single decay rate. These two points demonstrate the necessity of a more accurate description of the LT-GaAs material.

IV. MODEL

A. Hole and electron density calculation

To describe the carrier dynamics, we used a Shockley-Read-Hall model including thermal processes.[21,22] The rate equations concern an electron density in the conduction band n, a hole density in the valence band p, and a nonionized deep-donor density n_{DD}. Since the SRH-recombination is dominant in LT-GaAs, the band-to-band radiative recombination term is neglected here, as well as Auger recombination. The surface recombination term is also neglected, since the

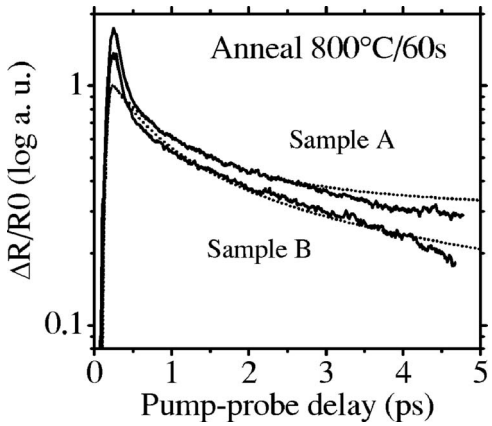

FIG. 4. Recorded transient reflectivity data for samples *A* and *B* annealed 800 °C/60 s (solid lines) and the corresponding calculated curves (dotted lines).

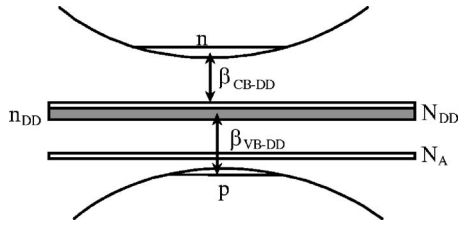

FIG. 5. Schematic energy bands illustrating the model parameters.

presence of the AlGaAs barriers prevents carrier leakage to the surface. The rate equations can be expressed as follows (see Fig. 5 for definitions):

$$\frac{dn}{dt} = \frac{I}{h\nu}\alpha - \beta_{\text{CB-DD}} n(N_{\text{DD}} - n_{\text{DD}}) + n_{\text{DD}}\beta^{\text{th}}_{\text{DD-CB}} \tag{1}$$

$$\frac{dn_{\text{DD}}}{dt} = -\beta_{\text{VB-DD}} n_{\text{DD}} p + \beta_{\text{CB-DD}} n(N_{\text{DD}} - n_{\text{DD}}) + \beta^{\text{th}}_{\text{DD-VB}}(N_{\text{DD}} - n_{\text{DD}}) - \beta^{\text{th}}_{\text{DD-CB}} n_{\text{DD}} \tag{2}$$

$$\frac{dp}{dt} = \frac{I}{h\nu}\alpha - \beta_{\text{VB-DD}} n_{\text{DD}} p + \beta^{th}_{\text{DD-VB}}(N_{\text{DD}} - n_{\text{DD}}) \tag{3}$$

where I is the time-dependent incident power density, $h\nu$ is the beam energy, α is the GaAs absorption coefficient at $h\nu$, $\beta_{\text{CB-DD}}$ is the electron-to-donor capture coefficient, $\beta_{\text{VB-DD}}$ is the hole capture coefficient, and $\beta^{\text{th}}_{\text{DD-CB}}$ and $\beta^{\text{th}}_{\text{DD-VB}}$ are the thermally activated detrapping coefficients, which read

$$\beta^{\text{th}}_{\text{DD-CB}} = \beta_{\text{DD-CB}} \frac{N_c}{2} e^{-E_{\text{DD}}/kT} \tag{4}$$

$$\beta^{\text{th}}_{\text{DD-VB}} = \beta_{\text{DD-VB}} 2N_v e^{-(E_G - E_{\text{DD}})/kT} \tag{5}$$

where N_c and N_v are the effective density of states in the conduction and valence bands, and E_{DD} is the energy distance between the DD band and the conduction band. The capture coefficients are of the form $\beta_{e,p} = \sigma_{e,p} . v_{e,p}$, where $\sigma_{e,p}$ is the capture cross section of the defect and $v_{e,p}$ is the electron (or hole) thermal velocity.

Following the model proposed by Look *et al.*,[22] we assumed that the position of the Fermi level is imposed by the compensation between N_A^*, the total density of incorporated acceptors, and the $N_{\text{DD}}+N_{\text{DS}}$ donors, where N_{DS} represents all shallower donors and N_{DD} represents the dominant deep-donor density. This is expressed by the following charge-balance equation:

$$n + (N_A^* - p_A) = p + (N_{\text{DD}} - n_{\text{DD}}) + (N_{\text{DS}} - n_{\text{DS}}). \tag{6}$$

The hole density remaining in the acceptor level and the electron density in the donor levels other than the deep one are denoted p_A and n_{DS}, respectively. We can write the net acceptor density as $N_A = N_A^* - N_{\text{DS}}$. The shallow donor levels close to the conduction band are supposed entirely ionized, i.e., $n_{\text{DS}} \ll N_{\text{DS}}$. Since the acceptor level, attributed to gallium vacancies and residual doping in the MBE reactor, lies just above the valence band, it follows that $p_A \ll N_A^*$, and p_A can be neglected in Eq. (6). In the absence of carriers in the bands, we get with these approximations $N_A = N_{\text{DD}} - n_{\text{DD}}$,

which means that the amount of empty deep-donor states is determined by the net acceptor concentration.

It should be noted that although the approximations $n_{DS} \ll N_{DS}$ and $p_A \ll N_A^*$ hold very well in the equilibrium state when the Fermi level is positioned at midgap in the deep-donor band, they become questionable under optical excitation. Indeed, we have estimated that each pulse corresponds to the creation of 7×10^{17} cm^{-3} electron-hole pairs. A free hole density of 7×10^{17} cm^{-3} at room temperature corresponds to a quasi-Fermi-level of holes situated about 60 meV above the valence-band edge. Such a free hole population would imply in thermal equilibrium a significant hole occupation of the acceptor levels with occupancy factors of ~0.9 for Ga vacancies and of ~0.2 for shallow *C* acceptors. In fact, in our *transient* experiments, we believe that our approximation still holds even at relatively high optical excitation and that we never achieve significant carrier populations in the shallow donor and acceptor levels. More precisely, we never achieve populations in the shallow levels that are not negligible compared to the populations of free electrons or free holes, since we initially generate nonequilibrium free carriers that are subsequently mostly captured by the dominant deep traps. This allows us to neglect p_A and n_{DS} in Eq. (6), also in the transient phase.

We also take into account in the model the effect of deep-donor absorption in the electron carrier density. This is done by replacing in Eqs. (1) and (3) the generation term $(I/h\nu)\alpha$ by $I/h\nu(\alpha+\alpha_{DD})$, where $\alpha_{DD}=\sigma_{DD}n_{DD}$, σ_{DD} being the trap absorption cross section. We assume an ultrafast cooling of the electrons to the bottom of the conduction band.

B. Refractive index and absorption coefficient calculation

After calculating the values of the carrier concentrations, we deduce the variation of the refractive index. For this, we calculate the variation of the absorption coefficient due to different effects: band-gap renormalization (BGR), band-filling (BF), and DD absorption. Following the data presented in Ref. 16, we neglected the free-carrier absorption: the variation of refraction index induced by the free-carrier absorption change, also called the plasma effect, is negative and proportional to the squared wavelength, but remains always negligible compared to BGR and BF effects for the relatively low photoexcited carrier densities used in this work. For the BGR, we take $\Delta E_{BGR}=c(n^{1/3}/m_e+p^{1/3}/m_{dh})$, where $m_{dh}=(m_{lh}^{3/2}+m_{hh}^{3/2})^{2/3}$ and c is a proportionality constant determined to fit the experimental results of Ref. 16. The resulting induced change in absorption reads $\Delta\alpha=\Delta\alpha_{BF}+\Delta\alpha_{BGR}+\Delta\alpha_{DD}$, with

$$\Delta\alpha_{BF}=\sum_{i=hh,lh}\frac{C_i}{E}\sqrt{E-E_g+\Delta E_{BGR}}[f_v(E_{vi})-f_c(E_{ci})-1] \tag{7}$$

$$\Delta\alpha_{BGR}=\sum_{i=hh,lh}\frac{C_i}{E}(\sqrt{E-E_g+\Delta E_{BGR}}-\sqrt{E-E_g}) \tag{8}$$

$$\Delta\alpha_{DD}=\sigma_{DD}\Delta n_{DD} \tag{9}$$

Δn_{DD} is the nonionized DD density change during the pump pulse, h and l refer to heavy and light holes, $C_{hh}=1.5\times10^{12}$ cm^{-1} s$^{-1/2}$ and $C_{lh}=7.8\times10^{11}$ cm^{-1} s$^{-1/2}$ (Ref. 16) (for GaAs), f_c and f_v are the Fermi-Dirac distribution functions, and $E_{chh,clh}$ and $E_{vhh,vlh}$ are the energies in the conduction and in the valence band corresponding to a photon energy $E=|E_{vhh,vlh}|+|E_{chh,clh}|$. Due to momentum conservation, we have only a unique set of values for $E_{vhh,vlh}$ and $E_{chh,clh}$, which read

$$E_{vhh,vlh}=(E_g-E)\left(\frac{m_e}{m_e+m_{hh,lh}}\right)-E_g \tag{10}$$

$$E_{chh,clh}=(E_g-E)\left(\frac{m_{hh,lh}}{m_e+m_{hh,lh}}\right) \tag{11}$$

Once the absorption change is calculated, we compute the real refractive index variation Δn_R using the Kramers-Kronig relation. The reflectivity R then reads

$$R=\frac{(n_R-1)^2-k_R^2}{(n_R+1)^2-k_R^2} \tag{12}$$

where k_R is the imaginary part of the complex refractive index (related to the absorption coefficient). The ΔR is calculated comparing the situation before and after the pump pulse. In all our simulations, we verified that the imaginary part is negligible compared to the real one, and thus the variation of the reflectivity ΔR is directly proportional to the variation of the real part of the refractive index, Δn_R. We did not attempt to model the initial fast thermalization and cooling process.

C. Fitting methodology

The method adopted to fit the experimental results is the following: according to Ref. 23 the deep-donor absorption cross section is fixed at $\sigma_{DD}=2\times10^{-16}$ cm^2 (which gives $\alpha_{DD}=5\times10^3$ cm^{-1} for $N_{DD}=2.5\times10^{19}$ cm^{-3}), and we have determined a unique best set of electron and hole cross-sections (σ_n and σ_p) for *all samples*. The values we found were $\sigma_n=6\times10^{-15}$ cm^2 and $\sigma_p=1\times10^{-17}$ cm^2, in close agreement with those reported in previous studies.[6,21] We should note that doing this, we assumed that the defects were the same for all samples (annealed or not). Also, it is important to underline that a slight degree of freedom arises from the normalization of each measured datum since the initial thermalization process, which defines the maximum value of the $\Delta R/R_0$ signal, is not calculated here.

In summary, the N_{DD} is given by the value measured by HR-XRD (when it can be measured) and we end up with one main single fitting parameter: N_A. By changing this value, we must be able to describe every observed behavior.

V. MODELING RESULTS

A. As-grown and 500 °C/60 s annealed samples

The calculated results of $\Delta R/R_0$ for the as-grown and 500 °C/60 s annealed samples are shown in Figs. 2(a) and

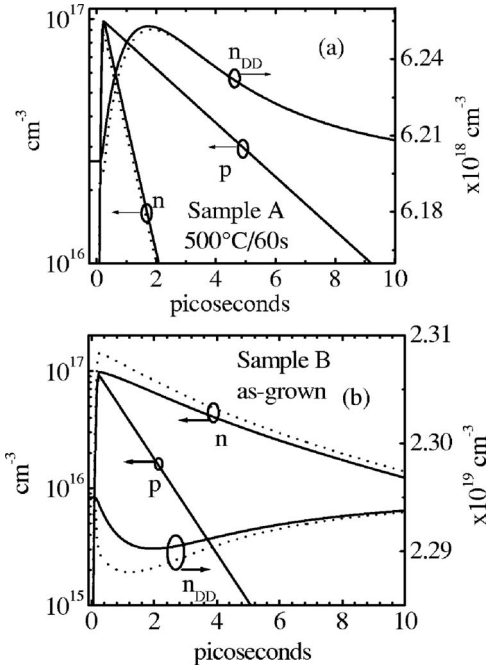

FIG. 6. Calculated carrier densities for the samples *A* annealed 500 °C/60 s (a) and *B* as-grown (b). Solid lines: without trap absorption; dotted: with trap absorption.

2(b): the recorded data before and after annealing are accurately described by the model. In Fig. 6 we plotted the calculated transient electron (n), hole (p), and ionized donor (n_{DD}) concentrations. We can see that for sample *A* annealed 500 °C/60 s [Fig. 6(a)], after the increase of n and p due to band-to-band absorption (first 0.1 ps), the electrons and holes are captured in the trap states, which give a net increase of n_{DD} (0–2 ps). This is due to the fact that the capture of electrons is more efficient than the capture of holes ($\beta_{CB\text{-}DD} \gg \beta_{VB\text{-}DD}$) and thus the electrons populate the empty deep-donor states faster than the holes. When the electrons are almost entirely captured (after ~2 ps), n_{DD} begins to decrease as the hole capture dominates the process.

For the as-grown sample *B* [Fig. 6(b)], the behavior of n and p is similar to the previous one, but with holes decreasing faster than electrons, and with a pronounced decrease of n_{DD} in the first ~2 ps. This is due to the very large value of N_{DD} combined with a low value of N_A: we have many more recombining states for the holes than for the electrons, and thus a faster decrease for holes than for electrons (even if $\beta_{CB\text{-}DD} \gg \beta_{VB\text{-}DD}$). We can note the initial concavity of the $n(t)$ curve, followed by a convexity for longer times, which reflects the emptying and filling of trap states.

As mentioned previously, a striking feature is that the signal decay rate remains the same (sample *A*) or even increases (sample *B*) after the 500 °C/60 s anneal. Our model relates this to a stabilized (sample *A*) or a slightly increased (sample *B*) value of N_A (see Table I). Such slight increases (stabilizations) of the acceptor concentration after low-temperature anneals have already been observed by Bardeleben *et al.* (electron paramagnetic resonance experiments)[24] and Liu *et al.* (magnetic circular dichroism experiments).[15] McIntosh *et al.*[7] also reported unchanged ΔR decay rates after 480 °C/520 °C anneals, which could be

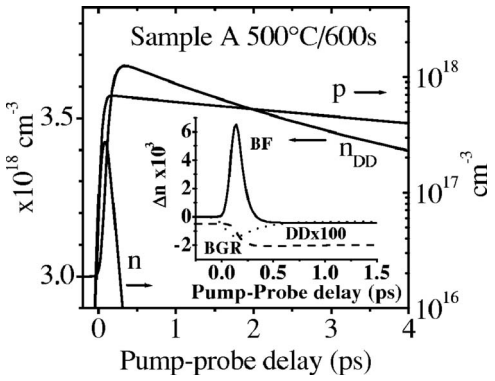

FIG. 7. Calculated hole, electron, and nonionized deep-donor populations for sample *A* annealed 500 °C/600 s. Inset: contributions of the BGR (dotted line), BF (solid line), and DD absorption (dashed line, ×100) to the Δn.

related, according to our model, to an unchanged N_A. We should also note that all authors observed, like us, an increase of the lifetime after higher-temperature anneals. All these results are coherent with our analysis.

Concerning the role of trap absorption, we calculated the different carrier populations for samples *A* and *B* taking into account this effect [dotted curves in Figs. 6(a) and 6(b)]. We can see that the trap absorption represents only a secondary correction, even if the effect is larger for the as-grown sample than for the annealed one, due to its higher amount of absorbing traps. Nevertheless, it must be stressed here that we have chosen only one trap absorption cross section for *all* samples in order to reduce the fitting parameters. But the possibility exists that the trap absorption cross section (σ_{DD} coefficient in our model), which determines the impact of DD absorption on the ΔR behavior, may not be the same for the as-grown and the annealed samples. This can be the case if we have, for example, different kinds of defects before and after annealing. Our only conclusion on this point is that the role of deep-donor absorption in the reflectivity transients is nearly negligible. This naturally implies that no firm data can be extracted from the set of experiments presented in this paper about the values of the deep-donor absorption cross section or even about the correctness of the use of a single cross section.

B. 500 °C/600 s annealed samples and negative transients

For the long annealed samples, we also obtained a good fit of the recorded data, including the negative transient (NT), only by tuning the N_A (see Fig. 3). The discrepancy for short times (<1 ps) is attributed to the fact that we do not calculate the thermalization process. In our modeling, the NTs appear to be related to large N_A[~$(6-7)\times10^{18}$ cm^{-3}] and N_{DD} values, which ensure a high amount of ionized DD, and therefore many more empty states for electrons than for holes. This leads to an extremely fast decrease of $n(t)$ compared to $p(t)$ (see calculations on Fig. 7), which gives an initial subpicosecond decay time of the reflectivity curve (associated with the decay of electrons), and then a slow nega-

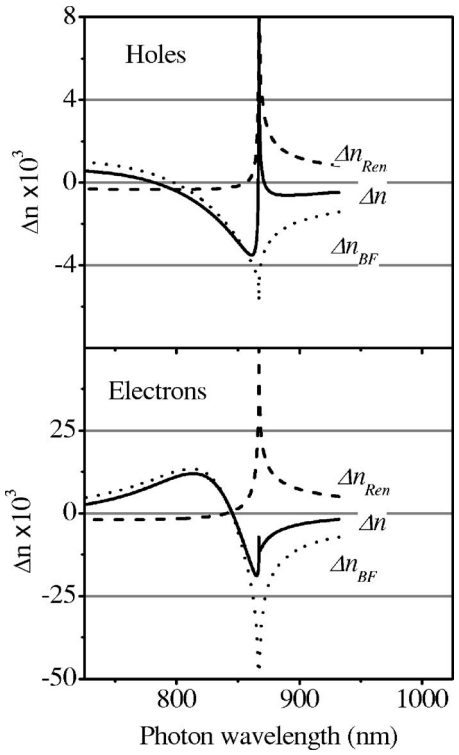

FIG. 8. Calculated Δn for electrons (we set $n=7\times10^{17}$ cm^{-3}, $p=0$) and holes (we set $n=0$, $p=7\times10^{17}$ cm^{-3}), as a function of the probe wavelength (solid lines), for the different contributions (BF, dotted and BGR, dashed). The Δn calculation takes into account the effects of the BF, BGR, and DD absorption. We remind that ΔR was found to be almost proportional to Δn.

tive signal, which is associated with the holes, as we will confirm by modeling IR transmission experiments (see below).

This interpretation explains why NTs have mostly been observed in the literature in samples with a high amount of N_{DD}.[9,10] Usually, the NTs disappear when the samples are annealed, i.e., when N_{DD} and N_A are reduced, as expected.

Figure 3 (inset) shows the $\Delta T/T_0$ IR data compared with the calculated hole population decrease. Following our calculations, since the electron population decreases in a subpicosecond time scale, the ~150 ps duration of the $\Delta T/T_0$ IR signal should be related to the remaining hole population (free-carrier absorption). Indeed, we can see that the decay rates of the $\Delta T/T_0$ IR signal and the calculated hole population are the same. This result reconfirms the validity of our analysis.

The relation between the hole population and the NTs is also confirmed by calculating the different contributions to Δn (which is directly proportional to ΔR) if we had only a population of electrons or only a population of holes (see Fig. 8). Indeed, we can see that the sign of the Δn curve for electrons becomes positive for $\lambda<840$ nm, while for the holes this happens only for $\lambda<780$ nm. The origin of that effect is related to the larger hole effective mass, which gives a different shape of the Δn versus λ curve and thus negative Δn at wavelengths far above the band gap. For the wavelength used in our experiments (around 810 nm), the NTs are therefore related to the holes, which confirms our previous conclusions. We can also note that this wavelength dependence can be employed to probe, for example, only the electron population (with a pump-probe wavelength of about 780 nm) and thus avoid the NTs.

Concerning the different contributions (BF, BGR, and DD), we can see in Fig. 8 that for all the wavelengths above the band gap, Δn roughly follows the dependence given by the BF, which is therefore the dominant effect. The calculations also show that the DD absorption contribution is negligible compared to the BF and BGR ones (see the inset of Fig. 7).

A striking feature of our data is that the NTs are mainly present in the 500 °C/600 s annealed samples. This is related to a strong increase of N_A after such a long anneal. We should note that strong increases of N_A after long, low-temperature anneals have already been observed by Fang and Look,[25,26] and attributed to the reaction $As_{Ga}\rightarrow V_{Ga}+As_i$. This reaction generates gallium vacancies, known as acceptors, and can explain the behavior we observed. It should be stressed here that it is likely that the conditions under which the strong increase of N_A could be observed depend critically on the initial (as-grown) state (in terms of N_{DD} and N_A) of the LT material.

Another interesting point is that our analysis implies that *p*-doped LT-GaAs should have a strong tendency to exhibit NTs (because N_A will be fixed at a very large value): in fact, photoreflectance studies at 800 nm on such layers[27] show the same NTs as ours. Another source of NTs could also be an important residual doping in the MBE reactor. This implies particularly that two materials grown on two different reactors at exactly the same temperature, growth rate, V/III ratio, and with the same amount of incorporated excess As can have different transient behaviors due to a different amount of incorporated residual acceptors.

C. Above 700 °C annealed samples

For the samples annealed at 700 and 800 °C/60 s, the DD concentration falls below the HRXRD detection limit, which is around 1×10^{18} cm^{-3}. On the other hand, the lower limit of N_{DD} is given by N_A, since Hall measurements show that these samples are always *n*-type. Once N_{DD} is fixed between these two limits, the calculations show that the transient reflectivity signal of samples annealed at 700 and 800 °C/60 s is mainly driven by N_A (which is quite low, see Table I). This is related to the sensitivity to the initial decay rate, which is related to the trapping of electrons in the empty DD states, which are fixed by N_A. Concerning the low values of N_A and N_{DD}, these are understandable since we expect a drastic reduction of point defects with increasing annealing temperatures.

However, although the presented model fits correctly the recorded $\Delta R/R_0$ signals of the 800 and 700 °C/60 s annealed samples, there is a slight discrepancy between the calculated and recorded values for long times (see, for example, Fig. 4, at ~5 ps). Indeed, the presented model may not be valid for these very high annealing temperatures ($T_A>700$ °C), where other processes can also play a significant role, such as recombination of carriers on As-precipitates[6,28,29] or a variation of the DD capture cross

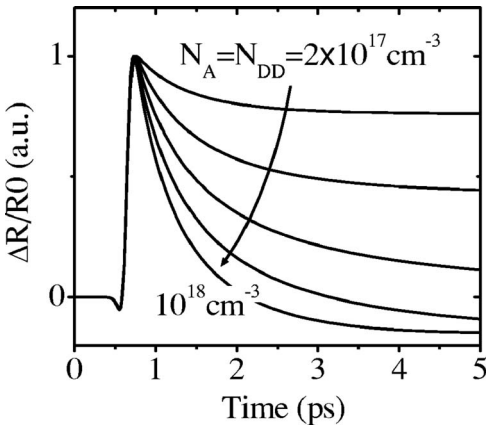

FIG. 9. Calculated transient reflectivity curves for an injection pulse of 7×10^{17} cm^{-3} electron-hole pairs and various values of $N_{DD}=N_A$ (ranging from 2×10^{17} to 10^{18} cm^{-3}).

section due to a change in the defect environment.[30] Gregory *et al.*[29] have introduced recombination on As-precipitates in a two-trap model and were able to satisfactorily explain the dependence of the carrier lifetime on annealing temperature for a sample with a very high As concentration. In this case, the As-precipitate effect on recombination was found to be predominant for high annealing temperatures.

The regime where $N_{DD}\sim N_A$ and $N_{DD}<10^{18}$ cm^{-3} is also interesting. In particular, it implies that (i) there are many more available DD states for electrons than for holes, and (ii) the amount of available electron states is on the order of the electron-hole injected density (7×10^{17} cm^{-3}). These two points imply a decrease of the electron contribution to the signal and a saturation of the DD states. Then, we would have a remaining small electron population in the CB, a hole population in the VB, and the DD states filled with electrons. Since the capture cross section of holes is smaller than that of electrons ($\beta_{CB\text{-}DD}\gg\beta_{VB\text{-}DD}$), we would end up with a situation in which the decrease of the residual electron population is driven by the hole recombination on the DD states.

We confirm these conclusions by calculating $\Delta R/R_0$ for different values of $N_{DD}=N_A$ (see Fig. 9). We can see that for high $N_{DD}=N_A$ values (i.e., higher than the electron-hole injected density of $\sim7\times10^{17}$ cm^{-3}), we have a hole-driven NT, which is understandable since the CB electron density is rapidly approaching zero and we end up with a signal depending on the hole contribution only. For low $N_{DD}=N_A$ values, the NT is replaced by a *positive* transient, which is indeed associated with the CB electron population, which decreases at a rate determined by the recombination of holes, since the DD states are saturated by electrons. Such DD saturation has already been suggested by other authors.[3]

D. Note on the accuracy of the extracted value of N_A

The precision of the values obtained with our fits is related to the precision of the capture cross sections of electrons and holes. For the samples without NTs, once these values are fixed, the uncertainty of N_A is quite low, less than ±10%. But for the fits involving NTs, since we do not calculate the thermalization process, and since it is difficult to normalize the measured and calculated data for comparison,

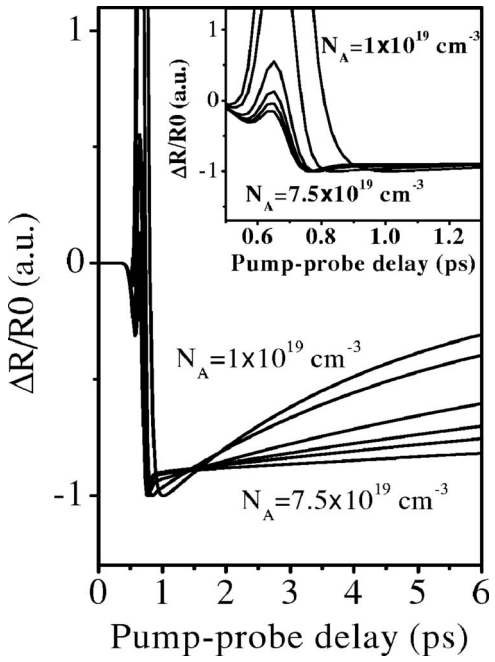

FIG. 10. Calculated transient reflectivity curves for an injection pulse of 7×10^{17} cm^{-3} and various values of N_A (1, 2.5, 5, 6, 6.5, and 7.5×10^{19} cm^{-3}, with fixed $N_{DD}=7.5\times10^{19}$ cm^{-3}). Inset: zoom of the 0.5–1.2 ps region.

the precision on N_A is deteriorated. This is demonstrated by the study shown in Fig. 10 (inset) concerning the influence of N_A on the NT. We can see that when N_A increases from 10^{19} to 7.5×10^{19} cm^{-3}, the signal becomes strictly negative, which complicates the normalization. We can also note here that, when N_A becomes small, the NT has a reduced recovery time (see Fig. 10), which is consistent with the fact that the available trapping states for holes are increased ($N_{DD}-N_A$ is larger).

Another source of uncertainty lies in the precise value of the injected carrier density, since it has a significant influence on the amplitude of the NT, and thus on the value of N_A. We recall here that the exact value of the probe wavelength also needs to be taken into account, as the amplitude of the NTs depends on the proximity of the wavelength to the band gap (see Fig. 8).

VI. CONCLUSION

We presented a comprehensive study of LT-GaAs materials annealed under different conditions, using pump-probe reflectivity and mid-IR transmission measurements. We interpreted all the obtained results using a Shockley-Read-Hall nonradiative recombination model, which introduces the deep-donor and the acceptor densities as the main fitting parameters.

From this study, we conclude the following. (i) In the model presented, the initial decay time of the electrons is mainly determined by the initial ionized trap density and, therefore, by the net acceptor density. (ii) The effect of trap absorption is more important for the weakly annealed samples, but in all cases it introduces only a slight correction of the carrier concentration dynamics. (iii) The negative transients observed in some samples are due to a slowly decreas-

ing hole population, which is related to a high amount of acceptors present in the matrix, which can be due either to gallium vacancies or to residual doping during the growth. (iv) For samples with high-temperature anneals (exceeding 700 °C), positive transients can be observed. In these samples, other recombination processes, such as recombination in As precipitates, would need to be taken into account to describe more accurately the observed results. (v) The existence and amplitude of the negative transients depend considerably on the probe wavelength and the pump power.

Optimum performance samples in terms of fast carrier capture and fast recovery are obtained in experimental conditions allowing incorporation of initial As excess concentrations of $(2-6)\times 10^{19}$ cm^{-3}, combined with short anneals at relatively low temperatures (60 s at 500 °C). Ongoing work is focused on the precise determination of N_{DD} and N_A directly from growth and annealing conditions to achieve precise control of the material properties and full prediction of the dynamic properties.

ACKNOWLEDGMENTS

We would like to thank Xavier Marcadet for his enriching comments and Renato Bisaro for his accurate HR-XRD measurements. Part of this work has been performed under the framework of the European EUCLID project "HELIOS," supported by the French MOD under DGA/DSP/STTC Contract No. 98390.

[1] J. L. Landman, C. G. Morgan, J. T. Schick, P. Papoulias, and A. Kumar, Phys. Rev. B **55**, 15581 (1997).
[2] D. C. Look, Z.-Q. Fang, J. R. Sizelove, and C. E. Stutz, Phys. Rev. Lett. **70**, 465 (1993).
[3] U. Siegner, R. Fluck, G. Zhang, and U. Keller, Appl. Phys. Lett. **69**, 2566 (1996).
[4] E. S. Harmon, M. R. Melloch, J. M. Woodall, D. D. Nolte, N. Otsuka, and C. L. Chang, Appl. Phys. Lett. **63**, 2248 (1993).
[5] J. K. Luo, H. Thomas, D. V. Morgan, and D. Westwood, Appl. Phys. Lett. **64**, 3614 (1994).
[6] A. J. Lochtefeld, M. R. Melloch, J. C. P. Chang, and E. S. Harmon, Appl. Phys. Lett. **69**, 1465 (1996).
[7] K. A. McIntosh, K. B. Nichols, S. Verghese, and E. R. Brown, Appl. Phys. Lett. **70**, 354 (1997).
[8] M. Stellmacher, J. Nagle, J. F. Lampin, P. Santoro, J. Vaneecloo, and A. Alexandrou, J. Appl. Phys. **88**, 6026 (2000).
[9] G. G. Lin, T. A. Liu, and C. L. Pan, Jpn. J. Appl. Phys., Part 1 **40**, 6239 (2001).
[10] S. Gregory, C. Baker, W. R. Tribe, M. J. Evans, H. E. Beere, E. H. Linfield, A. G. Davies, and M. Missous, Appl. Phys. Lett. **83**, 4199 (2003).
[11] S. Gupta, M. Y. Frankel, J. A. Valdmanis, J. F. Whitaker, G. A. Mourou, F. W. Smith, and A. R. Calawa, Appl. Phys. Lett. **59**, 3276 (1991).
[12] V. Ortiz, J. Nagle, and A. Alexandrou, Appl. Phys. Lett. **80**, 2505 (2002).
[13] R. Adomavicius, A. Krotkus, K. Bertulis, V. Sirutkaitis, R. Butkus, and A. Piskarskas, Appl. Phys. Lett. **83**, 5304 (2003).
[14] H. Eusèbe, J.-F. Roux, J.-L. Coutaz, and A. Krotkus, J. Appl. Phys. **98**, 033711 (2005).
[15] X. Liu, A. Prassad, W. M. Chen, A. Kurpiewski, A. Stoschek, Z. Liliental-Weber, and E. R. Weber, Appl. Phys. Lett. **65**, 3002 (1994).
[16] B. R. Bennett, R. A. Soref, and J. A. del Alamo, IEEE J. Quantum Electron. **26**, 113 (1990).
[17] M. K. Reed and M. K. Steiner Shepard, IEEE J. Quantum Electron. **32**, 1273 (1996).
[18] B. Golubovic and M. K. Reed, Opt. Lett. **23**, 1760 (1998).
[19] L. Pavesi and M. Guzzi, J. Appl. Phys. **75**, 4779 (1994).
[20] K.-F. G. Pfeiffer, S. Tautz, P. Kiesel, C. Steen, S. Malzer, and G. H. Döhler, Appl. Phys. Lett. **77**, 2349 (2000).
[21] M. Stellmacher, J. P. Schnell, D. Adam, and J. Nagle, Appl. Phys. Lett. **74**, 1239 (1999).
[22] D. C. Look, J. Appl. Phys. **70**, 3148 (1991).
[23] D. Streb, M. Ruff, S. U. Dankowski, P. Kiesel, M. Kneissl, S. Malzer, U. D. Keil, and G. H. Döhler, J. Vac. Sci. Technol. B **14**, 2275 (1996).
[24] H. J. von Bardeleben, M. O. Manasreh, D. C. Look, K. R. Evans, and C. E. Stutz, Phys. Rev. B **45**, 3372 (1992).
[25] Z.-Q. Fang and D. C. Look, Appl. Phys. Lett. **63**, 219 (1993).
[26] D. C. Look, D. C. Walters, G. D. Robinson, J. R. Sizelove, M. G. Mier, and C. E. Stutz, J. Appl. Phys. **74**, 306 (1993).
[27] W. K. Liu, D. I. Lubyshev, P. Specht, R. Zhao, E. R. Weber, J. Gebauer, A. J. SpringThorpe, R. W. Streater, S. Vijarnwannaluk, W. Songprakob, and R. Zallen, J. Vac. Sci. Technol. B **18**, 1594 (2000).
[28] P. A. Loukakos, C. Kalpouzos, I. E. Perakis, Z. Hatzopoulos, M. Sfendourakis, G. Kostantinidis, and C. Fotakis, J. Appl. Phys. **91**, 9863 (2002).
[29] I. S. Gregory, C. M. Tey, A. G. Cullis, M. J. Evans, H. E. Beere, and I. Farrer, Phys. Rev. B **73**, 195201 (2006).
[30] M. Stellmacher, R. Bisaro, P. Galtier, J. Nagle, K. Khirouni, and J. C. Bourgoin, Semicond. Sci. Technol. **16**, 440 (2001).